Study on critical speed of rotation in the multistage high speed centrifugal pumps rotors

Yabin Tian*, Anjie Hu

School of Civil Engineering and Architecture, Southwest University of Science and Technology, Mianyang 621010, China

Corresponding Author Email: tianyb2008@126.com

ABSTRACT

Apart from hydraulic performance, the critical rotate speed in wet operating condition (the liquid lubricant state) is an important parameter in the designing of the multistage high speed centrifugal pumps rotors. In this paper, the finite element dynamic model of the rotor in dry state (without lubricate) is analysed by the lubricant fluid applied to the disk and cylinder parts, and a resistance equation of the influence of the fluid is proposed based on the analysis. This resistance is then coupled into the dry state finite element dynamic model to obtain that of the wet state, which is considered as the fluid-solid coupled interaction. With this model, the study further studies the influence of several factors on the inherent frequency of the rotor, and simulates the bending and torsion formation of the physical model. Simulation results show that, when the fluid's influence is considered, the inherent frequency of the rotor is very different from that of the dry state, and hence this influence cannot be neglected in the designing of the rotor. These results are also verified by corresponding experiments.

1. INTRODUCTION

Throughout the main body of your paper, please follow these prescribed settings: 1) the font is mostly Times New Roman; 2) almost all the words are typed in 10 points except; 3) each line throughout the paper is single-spaced; 4) in most cases, 10 pts spacing shall be left above and below any heading, title, caption, formula equation, figure and table.

Actually, as mentioned in the abstract section, it will be rather easy to follow these rules as long as you just replace the "content" here without modifying the "form".

High speed multistage centrifugal pump has been extensively applied to petroleum, chemical industry, electric power, steel and other important industry areas. As an important industrial equipment, the pump units are getting larger and the corresponding speed is getting higher as the single-machine capacity increases. The pump's rotating speed now can easily exceed the first critical speed of the pump rotor, and can even approach the second and third critical speed. If the pump almost operates at critical speeds, the system will be unstable due to the sympathetic vibration, which will pose a formidable challenge to the steady operation of the pump. To avoid the problem of high speed operation, the critical speeds of the pump rotor must be precisely calculated when the high speed multistage centrifugal pump is designed.

The critical speeds of general rotor system are always calculated based on the dynamic characteristics of pump shaft and the oil film bearing. However, the dynamic characteristics of the rotor system are also influenced by the fluid (lubricating oil) within the system. As the operating speed getting higher, the effects of the fluid on the system become more obvious. Hence, to guarantee the computational precision, the fluid-structure interaction between the rotor system and the fluid must be considered in this case. [1]

Finite element dynamic mode has long been applied to the study of the rotor dynamic simulation since the 1970s, and has

been gradually developed in these years.[2] Compared with the original models which only considered the inertia movement's influence, the latest models are more closed to the engineer practice, since the factors such as rotational inertia, gyroscopic couple, axial load, internal and external anti-corrosion, shearing deformation, bearing spring, foundation elasticity, and so on are all discussed in these models. Moreover, the influence of the sliding bearing and sealing lubricate oil has been widely applied to the research of small circulation gap structure, which greatly improved the finite element dynamic mode. [3, 4]

However, some fatal factors are still neglected in these models. One of them is the problem of fluid-structure interaction of the circulating flow within a large gap. [5, 6] As we all know, the rotor system is immersed in the lubricating oil, which highly influences the motion of the rotor, especially when the rotating speed is very high. Large deviation will appear if this factor is neglected. Although the fluid-structure interaction is introduced in many commercial structural dynamics software, such as ADINA [7], ANSYS [8] etc., detailed models for a certain rotor system still need to be established. Scholars have done a lot of work to precisely predict the dynamic characteristics of the rotor system. Similar to the oil film bearing simulation, there are some scholars such as Tian Yabin [9], Antunes [10, 11], Sun Qiguo [12] studied the dynamic coefficient of the eccentric rotor when the fluid machinery soaked in the circulation fluid in the big gap. However, the fluid-structure interaction mechanism in the rotor system is much different from the oil film bearing, the dynamic coefficient is not appropriate for describing the dynamic characteristics of the rotate system. Scholars [13] also simulated the fluid-structure interaction by introducing the mass effects of the fluid. However, this method neglects the viscosity resistance of the fluid, which increases as the rotate speed goes up.

To precisely predict the critical speed of the pump rotor, in this paper, an improved fluid-structure interaction dealing method is applied to the finite element model. With this model, the effects of the fluid on critical speeds of the pump rotor is further numerically discussed [14, 15].

2. MATHEMATICAL MODELS

2.1 Dynamic model of the 'dry' multistage centrifugal pumps rotors

The model of 'dry' condition particularly refers to the rotor working condition without considering the fluid's influence. In this case the rotor system vibration equation is given by

$$M\ddot{u}(t) + Ku(t) = 0 \qquad (1)$$

where, M is the mass, K is the stiffness matrix, $\ddot{u}(t)$ and $u(t)$ are the finite element node acceleration and displacement respectively.

The solution of the above equation can be considered as a harmonic function, hence the following equation should be satisfied:

$$\det\left|K - \omega^2 M\right| = 0 \qquad (2)$$

With this equation, a serial combination of λi and ωi2 can be obtained. Each ωi2 refers to a feature vector $\{\phi_i\}$, which represents a certain format of free vibration. The inherent frequency can then be given by

$$f_i = \omega_i \big/ 2\pi \qquad (3)$$

Where f_i refers to the *ith* inherent frequency.

2.2 Gyroscopic effect

The gyroscopic effect on the rotor system can be expressed by the lagrange function, which is given by

$$L(u,\dot{u}) = \frac{\dot{u}^T M \dot{u}}{2} + \frac{\dot{u}^T G \dot{u}}{2} - \frac{u^T K u}{2} \qquad (4)$$

Where u represents n-dimensional displacement vector, and G$\dot{u}$is the gyroscopic term, in which G is a antisymmetric matrix. The dynamic equation of the rotor system can then be written as

$$M\ddot{u} + G\dot{u} + Ku = f_1(t) \qquad (5)$$

where $f_1(t)$ is the external force. The above equation is a second order differential equation. To solve it, the solution of the corresponding homogeneous equation must be obtained first.

With the solution of the homogeneous equation, the solution of the Eq. (5) can then be obtained by Duhamel integration as

$$M\ddot{u} + G\dot{u} + Ku = 0 \qquad (6)$$

2.3 Fluid-structure interaction force

The fluid-structure interaction force is influenced by the shape of the immersed structure and its vibration ways. For some typical vibration cases, the force can be calculated by some given equations. In this paper, the movement of rotor system can be regarded as the vibration of discs and cylinder in the fluid. The corresponding interaction forces are given as follows.

(1) Translational and corner vibration of discs
The vibration of a disc can be both translational and corner vibration. If a disc with radius R does the translational vibration in the direction parallel to its axis in the fluid, the interaction force between the fluid is given by

$$F = -m_{da}\ddot{x} - c_{da}\dot{x} \qquad (7)$$

where $m_{da} = 3\pi R^2 \sqrt{\frac{\eta\rho}{2\omega}}$, $c_{da} = 3\pi R(1 + \frac{2R}{3\delta})$, ρ and η represents the density and the viscosity of the fluid, and ω is the vibration frequency respectively, $\delta = \sqrt{\frac{2\eta}{\omega\rho}}$.

In the corner vibration cases, the fluid resistance moment on the disc is given by

$$M_0 = -i_{da}\ddot{\theta} g_{da}\dot{\theta} \qquad (8)$$

where $i_{da} = \frac{3\pi}{8} R^4 \sqrt{\frac{\eta\rho}{2\omega}}(1 + \frac{2R}{3\delta})$, $g_{da} = \frac{3\pi}{8}\eta R^3(1 + \frac{R}{\delta})$.

(2) Translational and corner vibration of cylinders
Cylinders also do the translational and corner vibration. If the cylinders do the translational vibration in the direction parallel to its axis in the fluid, the fluid resistance of the translation on the unit length can be written as follows:

$$q = -m_{sa}\ddot{x} - c_{sa}\dot{x} \qquad (9)$$

where

$$m_{sa} = 6\pi R \sqrt{\frac{\eta\rho}{2\omega}}(1 + \frac{R}{3\delta}), c_{sa} = 6\pi\eta(1 + \frac{R}{\delta}) \qquad (10)$$

In the cases of corner vibration, the resistance moment of fluid to the rotation centre corner is given by

$$dM_0 = -\left(m_{sa}\ddot{\theta} + c_{sa}\dot{\theta}\right) s^2 ds \qquad (11)$$

where, m_{sa} and c_{sa} are also given by Eq. (9).

2.4 The fluid-solid coupling model

To numerically analyze the influence of fluid on the rotor, these inter-action forces or moments above should be coupled with the motion equations.
(1) The equation of motion disc
According to the Eqs. (7) and (8), the nodal forces caused by fluid strength in the disk can be written as

$$Q_{1d}^F = -M_{da}\ddot{u}_{1d} - C_{da}\dot{u}_{1d}$$
$$Q_{2d}^F = -M_{da}\ddot{u}_{2d} - C_{da}\dot{u}_{2d} \qquad (12)$$

where, $M_{da} = \begin{pmatrix} m_{da} & 0 \\ 0 & i_{da}\end{pmatrix}$, $M_{da} = \begin{pmatrix} c_{da} & 0 \\ 0 & g_{da}\end{pmatrix}$

The motion equations of the disc are given as follows:

$$M_d\ddot{u}_{1d} + G_d\dot{u}_{2d} = Q_{1d} + Q_{1d}^F$$
$$M_d\ddot{u}_{2d} - G_d\dot{u}_{1d} = Q_{2d} + Q_{2d}^F \qquad (13)$$

with the Eq. (12), the Eq. (13) can be rewritten as

$$M_d^*\ddot{u}_{1d} + G_d\dot{u}_{2d} + C_d^*\dot{u}_{1d} = Q_{1d}$$
$$M_d^*\ddot{u}_{2d} - G_d\dot{u}_{1d} + C_d^*\dot{u}_{2d} = Q_{2d} \qquad (14)$$

where, $M_d^* = M_d + M_{da}$, $C_d^* = C_{da}$.

(2) The motion equation of shaft unit

1) The nodal forces caused by fluid resistance

According to the principles of virtual work and notes $x = [N]\{U_{1s}\}$, the following equations can be obtained:

$$\{\delta U_{1s}\}^T Q_{1s}^F = \int_l \delta x dF = \{\delta U_{1s}\}^T \int_l [N]^T dF \qquad (15)$$

and

$$Q_{1s}^F = \int_l [N]^T dF \qquad (16)$$

With notes $dF = qds$, the above equation can be rewritten as

$$Q_{1s}^F = -M_{sa}^F\ddot{u}_{1s} - C_{sa}^F\dot{u}_{1s} - K_{sa}^F u_{1s} \qquad (17)$$

where, $M_{sa}^F = \int_0^l m_{sa}[N]^T N ds$, $C_{sa}^F = \int_0^l c_{sa}[N]^T N ds$, $K_{sa}^F = \int_0^l k_{sa}[N]^T N ds$, the symmetry force is then given by

$$Q_{2s}^F = -M_{sa}^F\ddot{u}_{2s} - C_{sa}^F\dot{u}_{2s} - K_{sa}^F u_{2s} \qquad (18)$$

2) The nodal forces caused by fluid drag torque

Similarly, according to the principles of virtual work and notes $\theta = N'u_{1s}$, the following equations can be obtained:

$$\{\delta u_{1s}\}^T Q_{1s}^M = \int_l \delta\theta^T dM_0 = \{\delta u_{1s}\}^T \int_l [N']^T dM_0 \qquad (19)$$

and

$$Q_{1s}^M = \int_l [N']^T dM_0 \qquad (20)$$

with the Eqs. (13) and (14), we can get

$$Q_{1s}^M = -M_{sa}^M\ddot{u}_{1s} - C_{sa}^M\dot{u}_{1s} - K_{sa}^M u_{1s} \qquad (21)$$

where, $M_{sa}^F = \int_0^l m_{sa}[N']^T N's^2 ds$, $C_{sa}^F = \int_0^l c_{sa}[N']^T N's^2 ds$, $K_{sa}^F = \int_0^l k_{sa}[N']^T N's^2 ds$

the symmetry force is also given by

$$Q_{2s}^M = -M_{sa}^M\ddot{u}_{2s} - C_{sa}^M\dot{u}_{2s} - K_{sa}^M u_{2s} \qquad (22)$$

3) the shaft unit equations of motion considering the fluid.

$$M_s\ddot{u}_{1s} + G_s\dot{u}_{2s} + K_s u_{1s} = Q_{1s} + Q_{1s}^F + Q_{1s}^M$$
$$M_s\ddot{u}_{2s} - G_s\dot{u}_{1s} + K_s u_{2s} = Q_{2s} + Q_{2s}^F + Q_{2s}^M \qquad (23)$$

taking the equation (16), (17), (20), (21) into (23), and rearranging, we can get

$$M_s^*\ddot{u}_{1s} + G_s\dot{u}_{2s} + C_s^*\dot{u}_{1s} + K_s^* u_{1s} = Q_{1s}$$
$$M_s^*\ddot{u}_{2s} - G_s\dot{u}_{1s} + C_s^*\dot{u}_{2s} + K_s^* u_{2s} = Q_{2S} \qquad (24)$$

where, $M_s^* = M_s + M_{sa}^F + M_{sa}^M$, $C_s^* = C_{sa}^F + C_{sa}^M$, $K_s^* = K_{sa}^F + K_{sa}^M$.

(3) The motion equations of overall system

The motion equations of the overall system considering the fluid should have the following forms:

$$M_1^*\ddot{U}_1 + C_1^*\dot{U}_1 + G_1\dot{U}_2 + K_1^* U_1 = Q_1$$
$$M_1^*\ddot{U}_2 - G_1\dot{U}_1 + C_1^*\dot{U}_2 + K_1^* U_2 = Q_2 \qquad (25)$$

Or $M^*\ddot{U} + C^*\dot{U} + K^*U = Q$

where $M^* = \begin{pmatrix} M_1^* & 0 \\ 0 & M_1^*\end{pmatrix}$ is the system inertia matrix, $C^* = \begin{pmatrix} C_1^* & G_1 \\ G_1 & C_1^*\end{pmatrix}$ is the damping matrix, and $K^* = \begin{pmatrix} K_1^* & 0 \\ 0 & K_1^*\end{pmatrix}$ is the stiffness matrix. Other matrixes' definitions are given as follows: M_1^* is formatted by the shaft unit inertia matrix M_s^* and the disc cell inertia matrix M_d^*, C_1^* is formatted by the shaft unit damping matrix C_s^* and the disc unit damping matrix C_j^*, and K_1^* is formatted by the shaft unit element stiffness matrix K_s^* and the disc stiffness matrix K_j^*.

3. THE FINITE ELEMENTMODELIN ANSYS

The geometry model can be carried out in the finite element software ANSYS. The rotor system in this paper can be treated as a beam. There are mainly three kinds of beam elements in the software: Beam 3, Beam4, and Beam 188. Beam3 refers to the 2D beam elements, hence it can only be applied to 2D problem. Beam 4 and Beam 188 are both 3D beam elements, and the shape of the section need to be defined. However, the rotor system in the present work has a single shape of cylinder, and the application of the above methods complicate the issue. To simplify the model, this paper applied the pipe element

model PIPE 16 instead, which considered the rotor elements as solid pipes. Besides, the vane wheel was modelled by the mass elements and its rotational inertia was added on the elements. Other geometric details, such as rounding, gaskets, keyways and pores were neglected since they have little influence in the simulation. Stainless steel H410 (1Cr13) has been chosen as the material of the rotor, the properties of which are given as follows: poisson ratio of 0.3, density of 7850 Kg/m3, and young modulus of 200 GPa.

4. ANALYSIS OF THE ROTOR DYNAMICS

With the proposed model, the critical speeds of the rotor are numerically analyzed in the present work. To illustrate the influence of fluid (oil) on the system, this paper separately simulates the system performance with and without fluid. The 'dry condition' and 'wet condition' are adopted here to represent the cases of simulation results with and without fluid's effects.

The operating parameters of the high speed 10 stages centrifugal pump are given as follows: the rated speed is 7500 r/min, the shaft diameter is 85mm, the impeller is 215mm, the chief of the spindle is about 2353mm and the diameter of the support is 70mm.

The proposed model is applied to ANSYS by programming the parametric designing language (APDL), which is contained in ANSYS software. The gyro effects are also considered in the model since the rote speed is rather high for the rotor. By chosen the numerical model of each influential factors, this paper numerically analyzes these influences on the rotor vibration and critical speeds separately.

4.1 Influence of support stiffness on the critical speed

The influence of the support stiffness on the critical speed is given in table 1. As we can see from this table, the simulated critical speed increased with the support stiffness. The corresponding vibration shape is given in Fig. 1. As we can see in this figure, when the elastic support is taken into consideration in the model, the rigidity of the rotor decreased, which lead to the decrease of the critical speed. The value of the critical speed is about 5.6E+5N/m to 5.6E+7N/m in this case. Since the influence of the critical speed is so obvious, great errors may be made if it is neglected in the simulation. Only in the case of the rigidity support, such influence can be neglected.
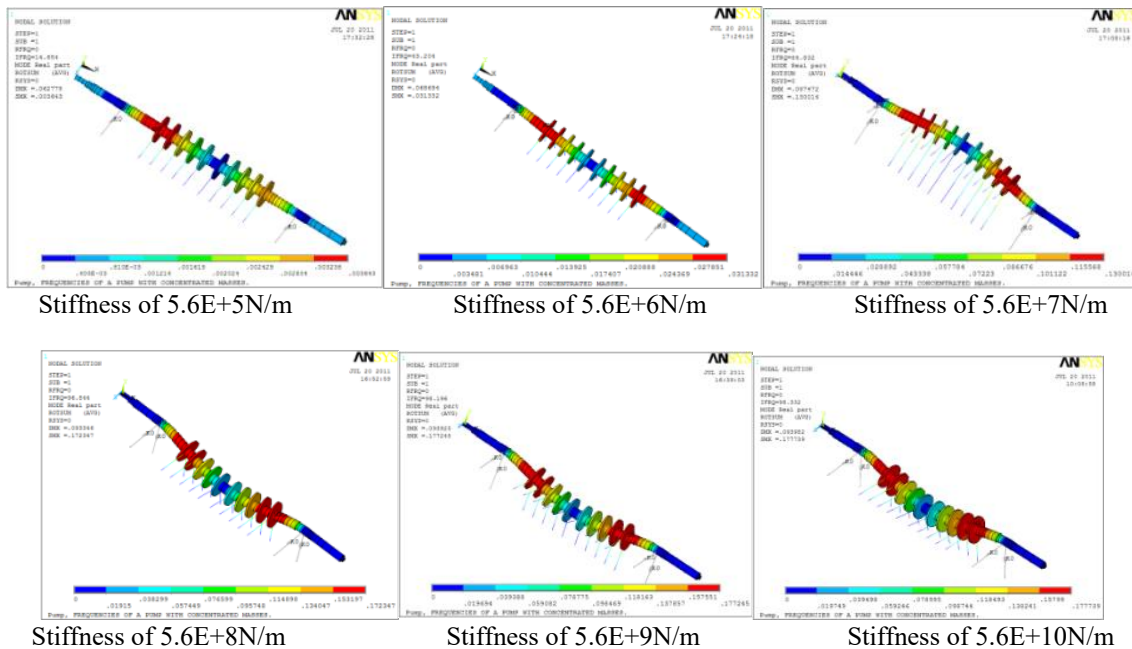

| Stiffness of 5.6E+5N/m | Stiffness of 5.6E+6N/m | Stiffness of 5.6E+7N/m |
| Stiffness of 5.6E+8N/m | Stiffness of 5.6E+9N/m | Stiffness of 5.6E+10N/m |

Figure 1. vibration shape with different support stiffness

Table 1. The inherent frequency with different support stiffness

Support stiffness	5.6E+5	5.6E+6	5.6E+7	5.6E+8	5.6E+9	5.6E+10
1st order frequency	14.65	43.20	84.83	96.84	98.20	98.33
2nd order frequency	50.57	80.94	184.66	266.39	276.78	277.71
3rd order frequency	171.89	181.96	251.73	291.24	295.28	295.78
4th order frequency	303.53	304.34	316.52	353.19	353.19	353.19

4.2 Influence of gyroscopic effect on the inherent frequency

The influence of the gyroscopic effect on the critical speed is given in table 2. It can be seen from this table that the critical rotor speed is reduced by the backward-precession while

added by the forward-precession. With the increase of the rotor speed, the influence of the precession gets more obvious. The influence of the gyroscopic effect on the vibration type is given by the figures 2- 4. It can be seen from these figures that the gyroscopic has little influence on the vibration type of the rotor.

Table 2. The inherent frequency with gyroscopic effect

Rotor speed r/min	1000		5000		7500		10000	
Direction	backward	forward	backward	forward	backward	forward	backward	forward
1st order frequency	96.76	96.93	96.42	97.26	96.22	97.47	96.01	97.68
2nd order frequency	266.12	266.66	265.06	267.72	264.39	268.39	263.72	269.05
3rd order frequency	291.12	291.36	290.62	291.86	290.31	292.18	290.01	292.49

Figure 2. The first order vibration type of the forward and backward precession
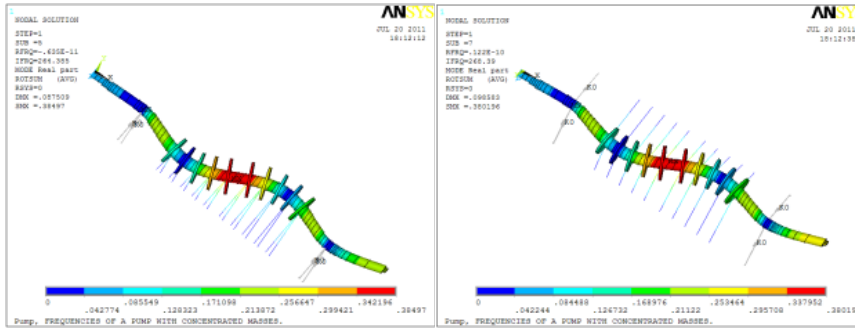

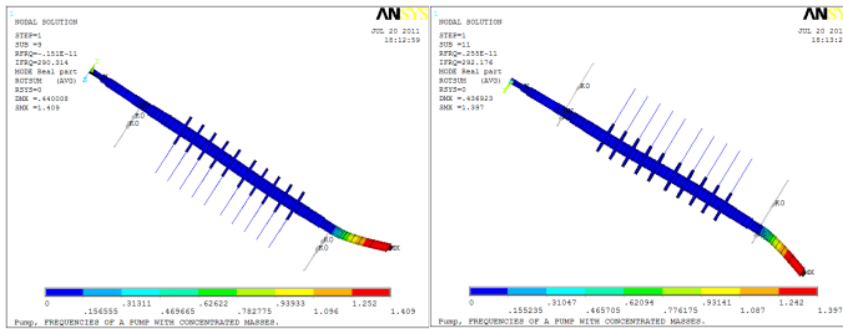**Figure 3.** The second order vibration type of the forward and backward precession

Figure 4. The third order vibration type of the forward and backward precession

4.3 Influence of fluid-structure interaction on the inherent frequency

On the base of the gyroscopic effect model, the influence of fluid-structure interaction on the critical speed is given in table 3. It can be seen from this table that the critical speed of each order is reduced. The reason of the decrease is that additional mass is added on the rotor by the fluid. However, the influence of the fluid on the speed is very limited since the additional mass is quite small, and this effect would be more obvious if the additional mass gets larger. Figs. 5-7 give the influence of the fluid on the vibration type, it can be seen from these figures that the vibration types change little compared with the cases without fluid-structure interaction.

Table 3. The inherent frequency with the fluid-structure interaction

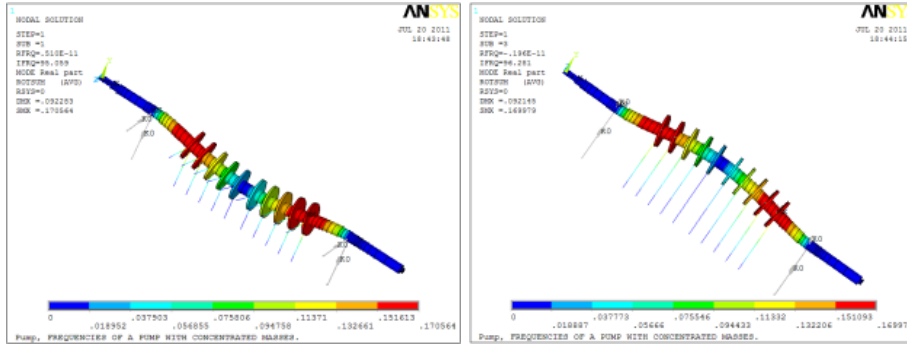| 1st order frequency		2nd order frequency		3rd order frequency	
backward	forward	backward	forward	backward	forward
95.06	96.28	261.48	265.43	290.18	292.00

Figure 5. The first order vibration type of the forward backward precession with the fluid-structure and interaction
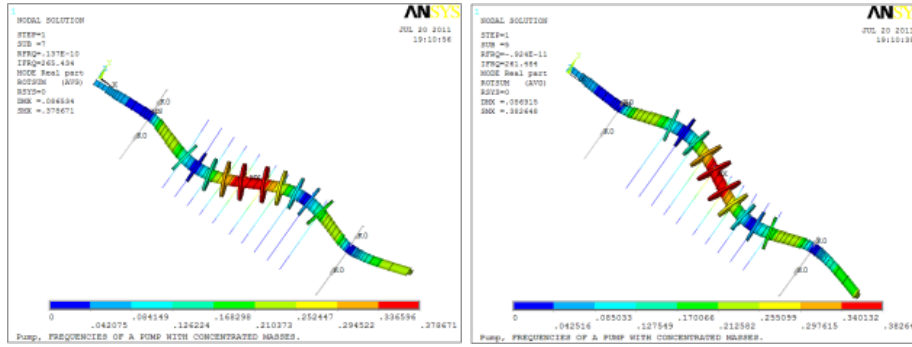

Figure 6. The first order vibration type of the forward and backward precession with the fluid-structure interaction
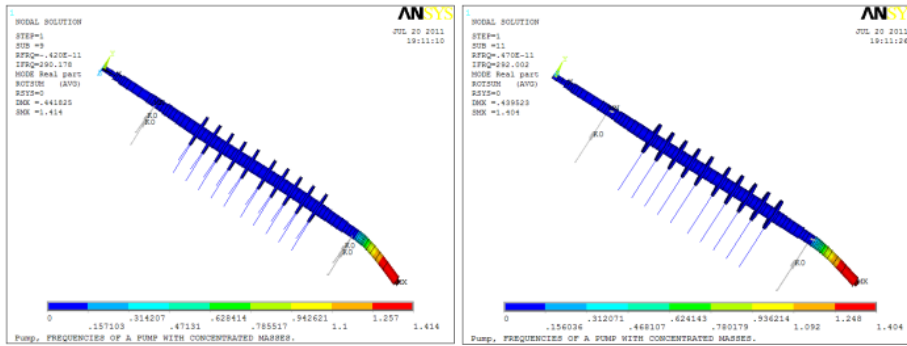

Figure 7. The first order vibration type of the forward and backward precession with the fluid-structure interaction

4.4 Influence of choma support stiffness on the inherent frequency

The influence of choma support stiffness on the critical speed is given in table 4.

Table 4. The inherent frequency with the choma stiffness

Choma stiffness		1.5E+5 N/m	1.5E+6 N/m	1.5E+7 N/m	1.5E+8 N/m
1st order	backward	97.12	114.00	220.65	289.47
	forward	98.34	115.22	221.85	291.13
2nd order	backward	262.18	268.24	288.64	353.19
	forward	266.12	272.10	290.31	(torsion mode)
3rd order	backward	290.20	290.48	326.42	366.27
	forward	292.03	292.39	330.40	367.91

It can be seen from this table that the vibration frequency of the rotor is added with the choma support stiffness. The effect of the choma on the rotor is similar to the effect of the support when its stiffness is constant, and this effect can be used to enhance the stability of the rotor, since it can increase the corresponding inherent frequency. Figs. 8-11 shows the corresponding vibration type under the effects of the choma support. It can be seen from these figures that the vibration type changes little when the stiffness of the choma increased from 1.5E+5N/m to 1.5E+6 N/m, while it changes obviously when the stiffness gets to 1.5E+7 N/m. The reason of these results is that the high stiffness choma can be viewed as an additional support which can restrain the transformation of the rotor.
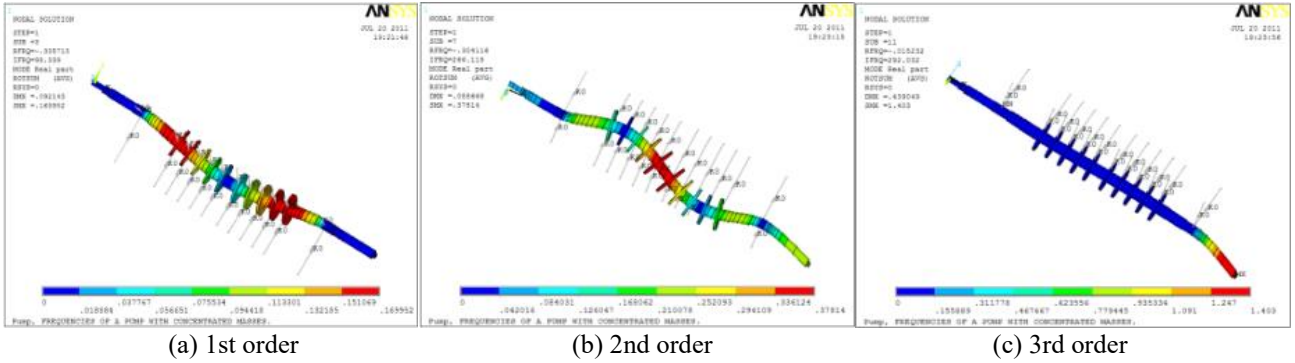
(a) 1st order   (b) 2nd order   (c) 3rd order

Figure 8. The first 3 orders vibration type of the forward and backward precession with the choma support stiffness of 1.5E+5 N/m

(a) 1st order   (b) 2nd order   (c) 3rd order

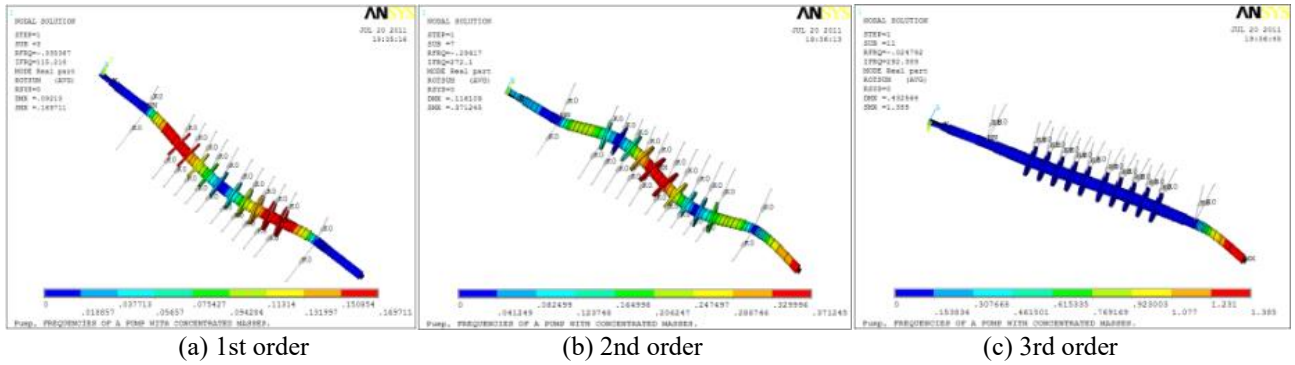**Figure 9.** The first 3 orders vibration type of the forward and backward precession with the choma support stiffness of 1.5E+6 N/m

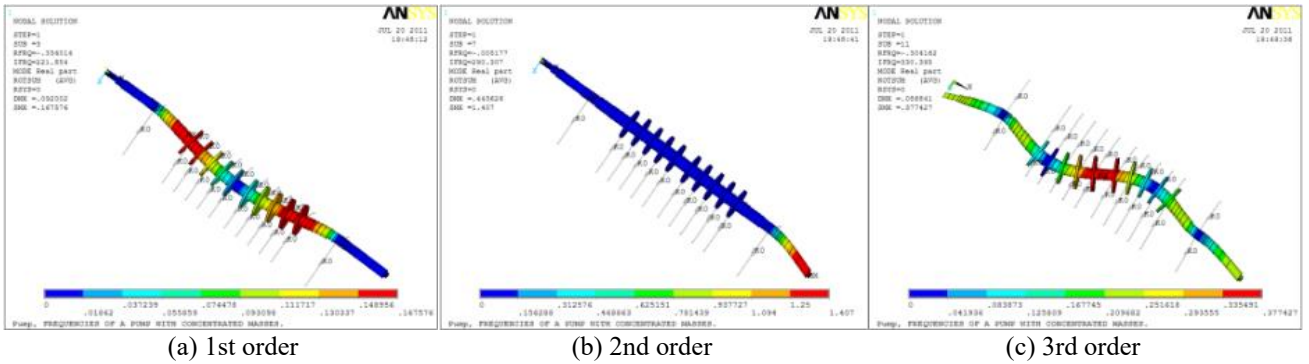
(a) 1st order   (b) 2nd order   (c) 3rd order

Figure 10. The first 3 orders vibration type of the forward and backward precession with the choma support stiffness of 1.5E+7 N/m

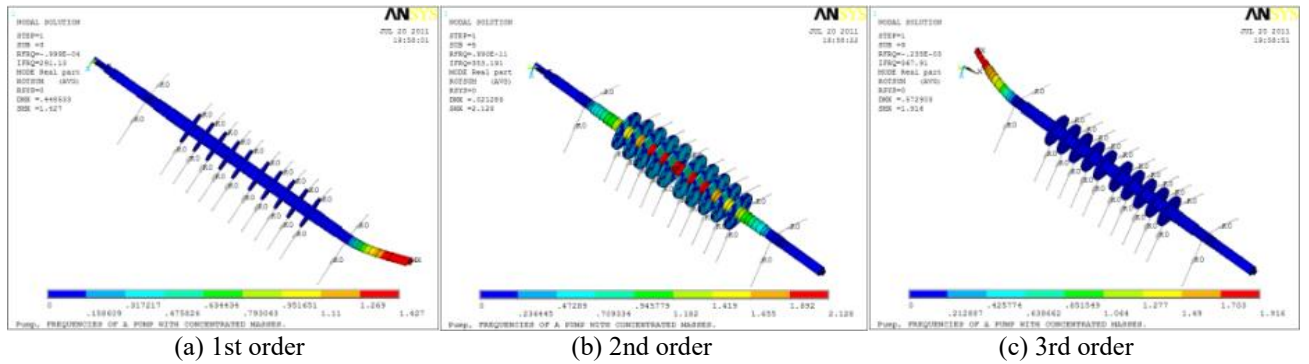(a) 1st order   (b) 2nd order   (c) 3rd order

Figure 11. The first 3 orders vibration type of the forward and backward precession with the choma support stiffness of 1.5E+8 N/m

4.5 Influence of additional axial stress on the inherent frequency

The influence of additional axial stress on the critical speed is given in table 5. It can be seen from this table that the inherent frequency also increased obviously under the influence of the axial stress. The corresponding vibration types are given in Fig. 12, from which it can be found that the vibration type changes a lot after the axial stress is considered,

and the bending vibration decreased and critical speed increased, which is beneficial to the stability of the rotor.

Table 5. The inherent frequency with the choma stiffness

1st order	2nd order	3rd order
269.16	292.94	353.19

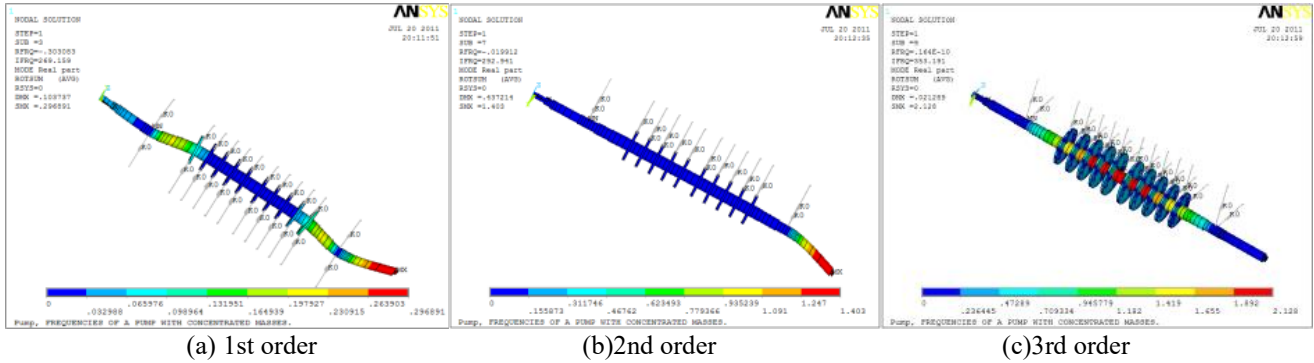(a) 1st order   (b)2nd order   (c)3rd order

Figure 12. The vibration types with the additional axial stress

In this section, the paper has numerically discussed the 5 main factors influencing the inherent frequency of the rotor. From these simulation results, it can be found that the influences of these factors are different, among these factors, the fluid-structure interaction, choma support, and axial stress have obvious effects on the operating character of the rotor: the inherent frequency of the 'wet' state is obviously higher than the 'dry' state; the choma support enhances the inherent frequency most when its stiffness is high; the axial stress influences not only the inherent frequency of the rotor but also its corresponding vibration type. The influences of these three factors are all good to the stability of the rotor, since they can enhance the stiffness of the rotor and restrain the deformation of the rotor

5. EXPERIMENT VERIFICATION

To verify the simulation results, the corresponding experiments are also carried out in this paper. The 3×8 3/4－10stg HSB high speed multistage centrifugal pump is chosen as the experiment object. And the dynamic signal acquisition system is made up of KD1005 piezoelectric built-in circuit (ICP) acceleration sensor, CYB11 type pressure transmitter, charge amplifier, pressure sensor preconditioning, and UT3208 collector. Each blade rotor is set with 4 collection points, and the sampling time is 3 min. The experiment results are given by the table 6.

Table 6. Experimental tested frequencies of the rotor system

1st order	2nd order	3rd order	4th order
267.33	291.12	352.41	366.23

It can be seen from this table that, compared with the simulation results, the critical rotor speed is a little lower in the experiment, while the inherent frequency is a little higher. This is mainly because the influencing factors of the experiment are more than that of simulation. All in all, the experiment results

are close to that of simulation, which verifies the simulation results.

6. CONCLUSIONS

This paper proposes a resistance equation of the influence of fluid on the high speed multistage centrifugal pump, and applies the equation to the simulation of the inherent frequency. In the simulation, several factors' influences are compared and discussed in detail. Finally, it verifies the simulation with the corresponding experiments. Following conclusions can be drawn based on the results:

(1) By integrating the role of fluid into the motion equation of the whole system to get the fluid-solid coupling finite element model of the rotor dynamics, the dynamics analysis of a real high speed multistage centrifugal pump rotor system can be done by the computer program with the finite element model. These analyses can verify the theory that fluid has an impact on dynamics performance of transversal subsystem.

(2) Simulation results show that the differences of the critical speed between dry and wet states in multistage centrifugal pump are obvious. Hence the effect of fluid-solid coupling on dynamic characteristics must be considered in calculation process.

(3) The dynamics analysis of high speed multistage centrifugal pump rotor shows that the effect of fluid on impeller can improve the stability of the rotor.

(4) The experiment results show a good consistence with the simulation results, which verifies the reliability of the present model.

REFERENCES

[1] Sun K, Li YP, Roy U. (2017). A PLM-based data analytics approach for improving product development lead time in an engineer-to-order manufacturing firm. Mathematical Modelling of Engineering Problems 4(2): 69-74.

[2] Pal M, Sarkar G, Barai RK, Roy T. (2017). Design of different reference model based model reference adaptive controller for inversed model non-minimum phase system. Mathematical Modelling of Engineering Problems 4(2): 75-79.

[3] Zaoui FZ, Hanifi HA, Abderahman LY, Mustapha MH, Abdelouahed T, Djamel O. (2017). Free vibration analysis of functionally graded beams using a higher-order shear deformation theory. Mathematical Modelling of Engineering Problems 4(1): 7-12.

[4] Kalla S, Marcoux H, De Champlain A. (2015). CFD approach for modeling high and low combustion in a natural draft residential wood log stove. International Journal of Heat and Technology 33(1): 33-38.

[5] Zhi Y, Min QF. (2015). Hei river flood risk analysis based on coupling hydrodynamic simulation of 1-D and 2-D simulations. International Journal of Heat and Technology 33(1): 47-54.

[6] Lv SJ, Feng MQ. (2015). Three-dimensional numerical simulation of flow in Daliushu reach of the yellow river. International Journal of Heat and Technology 33(1): 107-114.

[7] Zhang H, Zhang XL, Ji SH. (2003). Recent development of fluid2structure interaction capabilities in ADINA system. Journal of Computers and Structures 81(8211): 1071-1085.

[8] Sigrist JF, Laine C, Peseux B. (2002). ANSYS computation of fluid2structure interaction: Numerical and experimental analysis of an elastic plate in contact with a compressible heavy fluid. Journal De Physique IV 12(PR11): 137-144.

[9] Tian YB, Qi XY. (2013). Influence of axial stress on critical rotational speed of multistage centrifugal pump rotor. Transactions of the Chinese Society of Agricultural Machinery (44): 55-58, 88.

[10] Moreira M, Antunes J, Pina H. (2000). A theoretical model for nonlinear orbital motions of rotors under fluid confinement. Journal of Fluids and Structures (14): 635-668.

[11] Moreira M, Antunes J, Pina H. (2003). An improved linear model for rotors subject to dissipative annular flows. Journal of Fluids and Structures (17): 813-832.

[12] Sun QG, Yu L. (2000). Study of dynamic characteristics for fluid machine rotor immersed in annular liquid flow. Power Eengineeing 20(5): 906-910.

[13] Gu CH, Yao XL, Chen Q.F. (2001). Study on fluid-solid coupling dynamic characteristics for the component of hydraulic turbines. Large Electric Machine and Hydraulic Turbine (6): 47-52.

[14] Xu CD, Zhang HY, Zhang XQ, Han LW, Wang RR, Wen QY, Ding LY. (2015). Numerical simulation of the impact of unit commitment optimization and divergence angle on the flow pattern of forebay. International Journal of Heat and Technology 33(2): 91-96.

[15] Liu DW, Chen DH, Li Q, Xu X, Peng X. (2015). Investigation on the correlation of CFD and EFD results for a supercritical wing. International Journal of Heat and Technology 33(3): 19-26.

NOMENCLATURE

f_i	inherent frequency
G	antisymmetric matrix
G$\dot{u}$	the gyroscopic term
K	the stiffness matrix
M	the mass
U	displacement vector
u(t)	displacement
$\ddot{u}(t)$	the finite element node acceleration

Greek symbols

ρ	density, kg. m^3-1
η	the viscosity, m^2. s^{-1}